FATIGUE ANALYSIS OF BUS STRUCTURES

C.M. BRANCO* and J.A. FERREIRA**

The paper presents the main results of a fatigue analysis of welded joints in rectangular tubes used in bus structures. S-N and crack propagation data was obtained loading the specimens in plane bending in air at room temperature and at a loading frequency of 1410 cycles/min. Different steel grades were tested and their fatigue strength was compared.

A defect tolerance analysis was performed based on stress intensity computation and fatigue crack growth data. Defect or damage tolerance curves were obtained and compared with the experimental S-N curves. These curves can be used in the fatigue design of the structure.

INTRODUCTION

Bus structures are often subjected to dynamic loads leading to fatigue failures. In public transport vehicles the dynamic loads are transmited from the pavement to the structure causing fatigue in the welded joints of the tubes. The fatigue cracks usually initiate at the toes of fillet welds of T type connections made with rectangular thin walled tubes.

Welded rectangular thin walled sections with tube thicknesses ranging from 1.5 to 6 mm are extensively used as the main structural element in bus structures. These type of structures combine low weight with high values of the bending and torsion modulus. It is therefore possible to reduce the weight of the structure allowing an increasing load capacity in the vehicles and reducing the fuel consumption. However, fatigue failures should be avoided and therefore an appropriate fatigue design is required.

A considerable number of failures in bus structures have occured in the past in Portugal because fatigue loading was not taken into account in the design of the structure. The need for fatigue studies was recognized and the authors have initiated three years ago a testing programme in order to assess the fatigue behaviour of welded rectangular hollow sections used in bus structures. Some results were published elsewhere (1-4) and reported on the influence of tube thickness and weld surface finish. The crack propagation phase was studied with fracture mechanics methods applying the similarity approach and two simple crack propagation models. Fractographic observations were carried out using both optical and scanning microscopes and

* University of Minho, Braga, Portugal
** University of Coimbra, Coimbra, Portugal

as a result failure modes and crack initiation mechanisms were identified.

Research work in the field of fatigue of rectangular tubes has been extensively done in Holland by Wardenier (5,6) and in the USA by Stephens (7) Wardenier tests are in different types of tubular connections such as K, T and Y joints loaded in tension and bending. The influence of the geometry of the joint and welding location was assessed. However the size of the tubes was considerably greater than those used in bus structures, and moreover no study of the influence of weld geometry was performed. In (7) stress intensity solutions for surface cracks in square tubes subjected to torsion were obtained and in (8) similar results were obtained in rectangular tubes in bending. In these studies the similarity approach was applied for the K computation and that was based on compact tension specimen data obtained in specimens taken from the tube walls in the locations where the crack was propagating in the tubes. In (2) the authors found a reasonable agreement between their solution and Stephens one but only for cracks growing in the lateral sides.

Recently in Japan a detailed stress analysis study was published quoting structural stress concentration factor results obtained in several types of rectangular tubular connections (9). The finite element method was used but the geometry of the weld was not considered in the investigation. It is worth while to mention that in none of those papers defect tolerance and weld geometry was considered and these are fundamental parameters in any fatigue analysis of welded structures.

More work is being published in the field of fatigue of welded joints in circular tubular structures used in off-shore applications. Some of the latest results may be found in (10). In these structures conclusive proof now exists that Fracture Mechanics can be used to assess fatigue life and therefore its applicability to rectangular tubes should be studied and developed further as reported herein.

In the present paper a fatigue analysis methodology for welded joints in rectangular and square tubes of mild steel used in bus structures is presented. Fatigue design data was obtained in specimens representing the more critical details in the structure. The influence on fatigue life of material, tube and weld geometry is assessed theoretically and experimentally in some cases. A defect tolerance analysis was carried out using Fracture mechanics and the results were compared with the appropriate experimental data.

EXPERIMENTAL METHODS

The materials used were three mild steel grades St37-2,St44-2 and St 46-2 according to DIN 17100 specification. The steels are low carbon steels, containing 0.15% carbon in the St 37-2 grade and 0.16 to 0.18% carbon in the St 44-2 and St 46-2 grades respectively. The nominal dimensions of the tubes were 82x38x2 and 38x38x2 (height x width x thickness). These tubes are manufactured by cold bending of steel sheets with the same nominal thickness as the tube followed by resistance welding along the longitudinal direction. Hence the tubes have a welded longitudinal seam. The main mechanical properties obtained in tensile tests are presented in Table 1. Tensile tests were also carried out in plate specimens taken from the tube walls, but the results will not be reported here.

TABLE 1 - Mechanical properties of rectangular tubes of mild steel (DIN 17100)

Material	σ_{ys} (MPa)	σ_{UTS} (MPa)	ϵ_R (%)
St 37-2 Grade (82x38x2)	398	440	9.3
St 46-2 Grade (82x38x2)	370	428	33.8
St 46-2 Grade (38x38x2)	396	449	26.7
St 44-2 Grade (82x38x2)	381	458	---
St 44-2 Grade (40x40x2)	402	468	---

The fatigue specimens were tubes provided with fillet welded gusset plates simulating the critical detail in the structure where fatigue failure initiated. Fig. 1 shows the nominal dimensions of the specimen. The gusset plate shown is 3 mm thick and it is welded at the built-in end of the specimen in order to simulate the crack initiation point in service.Cantilever plane bending was chosen for the loading mode since that proved to be the appropriate loading node when checked by strain gauge readings in service. The same welding procedure and weld metal was used as in service. Thus this specimen is a full scale model of one of the more heavily stressed tubular T connections in the structure where fatigue failures have occured.

Fatigue testing was carried out in a specially build test rig with $\pm$ 20 kN maximum load capacity at the specimen free end (2). The top faces of the specimen were clamped at the gusset plate end (built-in end) as shown in Fig. 1. The weld toe region was outside the clamped ends and the load was applied at the other end of the tube using an eccentric and lever mechanism giving a constant deflection of the specimen free end. All the fatigue tests were performed in air, at room temperature with a loading frequency of 24 HZ and a stress ratio $R \approx 0$. The crack initiated in the weld toe of the upper gusset plate when the stress was tensile, propagated firstly through the upper part of the tube(upper rectangule of the cross section and then vertically through the lateral sides until it reached approximately the mid height of the specimen; then the test was stopped (see the sketch in Fig. 1).

In some tests crack length in the lateral sides was measured with a travelling microscope with an accuracy of 10^{-2} mm. Stroboscopic light was used for every crack length measurement and the sides of the tubes were carefully polished for a better crack tip observation.

Nominal stress was measured in the specimens using strain gauges bonded at locations 10 mm away from the weld toe and linearly extrapolated to the weld toe line. At the strain gauge location there is no stress concentration effect of the weld and this was confirmed by the finite element calculations. Hence the nominal stress at the weld toe was used to plot the

S-N data and the stress was monitored during the fatigue tests.

RESULTS AND DISCUSSION

Since crack propagated first in the upper part of the tube followed by propagation in the lateral sides it was decided to carry out the stress intensity factor computation separately for both parts. In the upper part, the K values were obtained numericaly applying the finite element method while for the lateral sides the similarity approach and an available K solution were applied.

Stress intensity factor computation in the upper part of the tubes

The stress intensity factor formulation for the upper part of the tubes (horizontal element) was computed based on the Albrecht method (11). This method is specially suited for welded joints and stress concentration geometries and is simple and quick to apply. In most practical cases the solutions derived for K are sufficiently accurate.

It is known that in welded joints there is always a stress gradient in the weld toe section. Hence the stress intensity factor may be obtained using the equation

$$K = M_k \frac{K'}{\phi} \qquad (1)$$

where ϕ is the complete second order elliptic integral ($\phi = 1$ for a continuous crack), K' is the stress intensity factor for a similar geometry without the weld and assuming a constant stress distribution along the thickness direction, and M_k is a magnifying factor taking due respect of the stress non-uniformity in the weld region. M_k is equal to the stress concentration factor when the crack length is zero and can be computed knowing the distribution of stress along the crack line and substituting these stress values in the M_k equation derived in (11).

For the specimen shown in Figure 1 and in the upper part of the tube subjected to cantilever bending, an approximate stress distribution can be assumed considering an uniform nominal tensile stress in the tube wall. This is approximately true due to the very small thickness of the tube walls. The stress distribution along the tube thickness was obtained with finite element method. Figure 2 shows the mesh used with eight node 2D isoparametric elements having two degrees of freedom in each node. In this figure B is the tube thickness, LG is the weld leg length and B_1 is the gusset plate thickness. Since an uniform tensile stress was required the loads were applied in tension in the nodes 116 to 124, and the built-in condition at the other end of the specimen was achieved by constraining the displacement in the nodes along the line 1 to 13.

M_k values were obtained for values of B = 2,3 and 4 mm, B_1 = 3 and 6 mm and LG = 6,12 and 20 mm. Table 2 presents the entire set of results for M_k as a function of a/B and these can be fitted accurately by a power law equation

$$M_k = p/(a/B)^q \qquad (2)$$

where p and q are dependent on B, B_1 and LG and the values are given in Table 2. The correlation coefficients for equation (2) are also quoted in the same table thus confirming the validity of equation (2).

TABLE 2 - Values of M_k in the upper part of the tubes ($M_k = p/(a/B)^q$)

B_1	3	3	3	6	6	6	3	3	3	6	6	6
B	2	3	4	2	3	4	2	3	4	2	3	4
LG	6	6	6	12	12	12	20	20	20	40	40	40
a/B	M_k	M_k	M_k	M_k	M_k	M_k	M_k	M_k	M_k	M_k	M_k	M_k
.01126	1.443	1.483	1.503	1.469	1.503	1.532	1.167	1.171	1.177	1.147	1.20	1.20
.05	1.214	1.211	1.194	1.215	1.197	1.186	1.087	1.079	1.077	1.10	1.088	1.0[illegible]
.08873	1.10	1.092	1.084	1.093	1.085	1.078	1.043	1.037	1.038	1.055	1.043	1.0[illegible]
.12255	1.044	1.037	1.033	1.042	1.034	1.037	1.021	1.017	1.019	1.028	1.022	1.0[illegible]
q	.1344	.1443	.1577	.1438	.1556	.1657	.0556	.0588	.0606	.0632	.0676	.0[illegible]
p	.7965	.7829	.7416	.7756	.7478	.7262	.9124	.9005	.897	.9038	.8852	.8[illegible]
Correlation coefficient	.994	.996	.999	.997	.999	.999	.996	.999	.999	.997	.999	.999

The stress concentration factors, $K_t = (M_k)_{a/B = 0}$ at the weld toe (point A in Fig. 2) were taken from Table 2 and its variation with tube thickness for the different weld geometries considered in Table 2 is shown in Figure 3. It is seen that the stress concentration factor increases when the weld leg length decreases and increases also with the gusset plate thickness. However the K_t values are not very high (range between 1.2 and 1.7). Photoelastic tests are in progress to establish a comparison of K_t values obtained by the two methods.

The computed stress values at the element nodes showed that for a/B values greater than 0.12 to 0.18 the stress values are very close to the nominal stress in the tube wall. Hence the stress gradient at the weld toe is rather localized and confined to the points situated at a distance less than 0.12 to 0.18 B. Then the equations for the stress intensity factor are

$$K = M_k(1.122-0.561\alpha-0.205\alpha^2+0.471\alpha^3-0.19\alpha^4)\sigma\sqrt{\pi a} = M_k K' \qquad (3)$$

and $K = K'$ when $M_k = 1$ for $0.12 \div 0.18 < a/B < 0.65$

In these equations $\alpha = a/B$, and for K' the Tada et al (12) solution for a single edge crack in a finite width plate in tension was taken. The M_k values are those given in equation (2) with the values of p and q taken from Table 2. ϕ was taken equal to 1 because the fractographic analysis revealed very shallow cracks growing from the tube corners (values of the ratio a/2c less than 0.2).

As the stress intensity values depend on the values of M_k it will be seen from the results given in Table 2 that K increases with tube thickness and decreases with increasing leg length following the same trend as the stress concentration factor results.

Fatigue crack propagation and stress intensity factor computation in the lateral sides of the tubes

Crack propagation in the lateral sides was measured during fatigue tests with precracked tubes in order to compare the crack growth behaviour of the steels and obtain data for the stress intensity computation. Typical plots crack length a in the vertical direction against number of cycles are plotted in Figs. 4 and 5. The results in Fig. 4 are for higher nominal stresses than Fig. 5. It is seen that the fatigue crack growth rate in the lateral

sides increases with the number of cycles and the applied stress and it is higher in the St 46-2 tubes compared with the St 44-2. Crack length values below 2 mm were not obtained since these occured in the upper part of the tube where no experimental observation was possible.

Other objective of these tests was to eliminate the crack initiation phase. Therefore the tubes whose results are plotted in Figs. 4 and 5 were provided with 0.65 mm deep notches at the corner. The notch was severe enough to initiate the crack after a very small number of cycles and that can be confirmed by the results shown in Figs. 4 and 5. However fatigue crack growth measurements in plain specimens (not precracked) revealed a significant crack initiation phase for low applied stresses (3,4).

The S-N curves for the 0.65 mm deep precracked tubes (rectangular and square) in the St 46-2 and St 44-2 steels are plotted in Fig. 6. Two curves were obtained, one for the 82x38x2 tubes and the other for the square ones (38x38x2). No influence of steel grade was found and only the height of the tube has influenced the S-N curve. Hence fatigue life is greater in the rectangular tubes due to the fact that the crack has to travel a bigger distance in the rectangular tubes before final failure occurs at the mid height of the tube.

S-N data was obtained in the plain welded tubes. The range of fatigue lifes is from 5×10^4 cycles to 10^7 cycles and in some tests fatigue failure did not occured. These results will be analysed later in the paper and here only a discussion about the variation of the nominal stress during the test will be done. Hence Fig.7 shows typical plots nominal stress against number of cycles in the strain gauge location indicated in Fig. 1 Nominal stress (stress in the outerfibre subjected to tension) remained practically constant while no crack was initiated in the upper part of the tube(usually at the tube corner near the strain gauges).This was followed by a slight increase in stress during crack propagation in the upper part of the tube and finally the stress in the outer fibre decreased sharply as the crack was propagating in the lateral sides. However the decrease in stress only occured when the crack was long,very near the end of the test. Hence it is accurate enough to consider a constant nominal stress in the specimen throughout the fatigue life.

The S-N curves of the precracked tubes (Fig. 6) were obtained by linear regression of the experimental results.

Assuming that fatigue life is crack propagation only, which is approximately true in this case, then the slopes of the S-N curves plotted in Fig. 6 are equal to the exponent m of Paris law. The constant C may be obtained by the following equation proposed by Gurney (13)

$$C = 1.315 \times 10^{-4} / 895.4^{m} \qquad (4)$$

Hence the values of m and C are

$m = 4.26$ and $C = 3.494 \times 10^{-17}$ for the rectangular tubes

$m = 4.68$ and $C = 2.01 \times 10^{-18}$ for the square tubes

These values of m are in close agreement with those of da/dN, ΔK curves obtained in fatigue crack propagation tests of centre cracked specimens in tension (14) .These specimens were taken from the tube walls and the crack was propagating in the same direction as in the tubes (14). Hence it appears that the method used herein for the determination of m is accurate and

has the advantage of being faster, more economical and easier than the one based on the determination of the da/dN, ΔK curve of the material.

Calculation of stress intensity factor in the lateral sides of the tubes

Two methods were used to obtain a K formulation for the lateral sides of the tubes. The first one is the Murakami (15) solution for a crack in the width direction of a rectangular cross section bar subjected to cantilever or plane bending. In the present study the width of the specimen was taken as equivalent to the tube height since the tube is built-in. The equation for K is

$$K = \sigma \sqrt{h} \quad \sqrt{\Pi \alpha} \quad (0.7857\alpha^2 + 0.6186\alpha + 0.862) \qquad (5)$$

where $\alpha = a/h$, h is the height of the tube and σ is the nominal stress at the weld toe line as defined before.

K values were also obtained applying the similarity approach and using the fatigue crack propagation data refered in the previous section (Figs.4 and 5).The equation to calculate the geometrical factor $Y = f(a/h)$ in the stress intensity equation may be expressed as (3)

$$Y = f(a/h) = \frac{1}{\sigma \sqrt{\Pi h}} \left(\frac{1}{C} \quad \frac{da}{dN} \right)^{1/m} \qquad (6)$$

with the values of m and C given above. From the (a,N) data obtained in the tubes (see Figs. 4 and 5 for examples) the da/dN equation was obtained in each specimen by numerical differentiation with the best fit second order polynomial. Hence f(a/h) can be computed in each specimen for a particular value of a (a/h) substituting in the above equation the da/dN value for that value of a (a/h) taken from the da/dN equation in each specimen.

For the St 46-2 steel Fig. 8 shows the plot f(a/h) against a/h obtained in the rectangular tubes and Fig. 9 is a similar plot for the square tubes. The data shown was obtained in five rectangular specimens and four square specimens. It is seen that f(a/h) increases with the crack lenght for values of a/h between 0.05 and 0.5 approximately. Crack propagation for values of a/h below 0.05 was not considered because it does not occur in the lateral sides. For a/h values above 0.5 crack growth rate is usually above 10^{-3} mm/cycle and the function f(a/h) has little practical interest in that region. Also the failure in the tubes was taken when the crack reached mid height of the specimen. A fourth order polynominal produced the best fit for the data points in Figs. 8 and 9 and the equations for f(a/h) are

Rectangular tubes (82x38x2)

$$f(\alpha) = 0.2162 + 2.231\alpha - 12.214\alpha^2 + 30.541\alpha^3 - 26.985\alpha^4 \qquad (7a)$$

Square tubes (38x38x2)

$$f(\alpha) = 0.2632 + 1.848\alpha - 6.172\alpha^2 + 10.171\alpha^3 - 6.418\alpha^4 \qquad (7b)$$

Therefore the stress intensity factor may be computed in the tubes with the following equations

(i) Rectangular tubes 82x38x2 ; LG = 6 mm and B_1 = 3 mm

$$K = 0.7965\ \alpha^{-0.0988} \times K' \qquad \text{for } \alpha = a/B < 0.184 \qquad (8a)$$

$$K = K' \qquad \text{for } 0.184 < a/B < 0.65 \qquad (8b)$$

and

$$K = \sigma\sqrt{h}\,\sqrt{\Pi\alpha}(0.2162+2.231\alpha-12.214\alpha^2+30.541\alpha^3-26.985\alpha^4) \qquad \alpha>B/h \quad (8c)$$

or $$K = \sigma\sqrt{h}\,\sqrt{\Pi\alpha}(0.7857\alpha^2+0.6186\alpha+0.862) \qquad \alpha>B/h \quad (8c)$$

(ii) Square tubes 38x38x2; LG=6 mm and B_1= 3mm

$$K = 0.7965\alpha^{-0.0988} \times K' \qquad \text{for } a/B < 0.184 \qquad (9a)$$

$$K = K' \qquad \text{for } 0.184 < a/B < 0.65 \qquad (9b)$$

and

$$K = \sigma\sqrt{h}\,\sqrt{\Pi\alpha}\,(0.2632+1.845\alpha-6.172\alpha^2+10.171\alpha^3-6.418\alpha^4) \qquad \alpha>B/h$$

or $$K = \sigma\sqrt{h}\,\sqrt{\Pi\alpha}(0.7857\alpha^2+0.6186\alpha+0.862) \qquad (9c) \qquad \alpha>B/h$$

Fractographic analysis

Scanning and optical microscope photographs of fracture surfaces were taken in order to detect crack initiation points and modes of crack propagation. Two examples can be seen in Figs. 10 and 11. Fig. 10 shows the entire top left corner of a St 46-2 tube tested at a nominal stress of 232 MPa. The picture covers all the tube thickness, the weld toe and weld metal. The cracks have initiated both at the weld toe and at the inner surface of the tube. Propagation took place in the horizontal and vertical directions in a similar pattern. This was the more often found crack initiation and propagation mode and that fits, so far as the crack propagation in the vertical direction is concerned, rather well with the theoretical model used in the present work. In Fig. 10 an internal flaw was observed (cleavage) probably due to HAZ cracking or material inhomogenity.

Fig. 11 with a higher magnification than Fig. 10 was taken in the lateral side of a rectangular tube of St 46-2 steel tested at a very low stress level (154 MPa). Crack propagation is by mixed mode both transgranular and intergranular.

Two grains of the material are visible in the photograph and within the grains striation formation is indicated despite the fact that these could only be seen with a higher magnification. This mixed mode was generally found for low stress levels only. For higher stress levels crack propagation was mainly intergranular.

Defect tolerance analysis and comparison with S-N data

Crack propagation S-N curves as a function of initial flaw size were derived so that a defect tolerance programme can be developed for this type of welded joints. The data can therefore be used in any defect tolerance analysis in bus structures since the results apply to the more critical weld detail in the structure.

The crack propagation S-N curves were the integration of the Paris law equation substituting the K values by equations (8) and (9). The resulting equation for the total number of cycles of crack propagation was

$$N_t = N_1 + N_2 + N_3 = \frac{1}{C\sigma^m}\left[\frac{(I_1+I_2)}{B^{\frac{m}{2}-1}} + \frac{I_3}{h^{\frac{m}{2}-1}}\right] \qquad (10)$$

where N_1, N_2 and N_3 are the number of cycles of crack propagation for the three terms of the stress intensity equations respectively ($a/B<0.184$; $0.184<a/B<0.65$ and $\alpha>B/h$) and I_1, I_2 and I_3 are the crack propagation integrals for the same stages and given by the equations

$$I_1 = \int_{\alpha_i}^{\alpha_o} \frac{1}{\left(\sqrt{\Pi\alpha}\;M_k\;Y\right)^m}\,d\alpha \qquad \text{where } \alpha_o=0.184 \text{ and } \alpha_i=a_i/B$$

$$I_2=\int_{\alpha_o}^{1} \frac{1}{\left(\sqrt{\Pi\alpha}\;Y\right)^m}\,d\alpha \quad \text{and} \quad I_3=\int_{B/h}^{0.5} \frac{1}{\left(\sqrt{\Pi}\;f(\alpha)\right)^m}\,d\alpha \qquad (11a,b,c)$$

In these equations Y is the geometrical factor for the K' equation (Tada solution) and $f(\alpha)$ is either the Murakami geometrical factor(equation 5) or the functions given by equations 7a) and 7b).

The integrations were carried out as a function of a_i, the initial crack size at the weld toe in the tube wall, and in the thickness direction. The values of a_i=0.1; 0.2 and 0.65 mm were selected since the first two represent typical flaw sizes in these welds, as shown by nondestructive inspection procedures in the structure, and the latter one is the initial flaw size for the experimental results plotted in Fig.6. Bigger initial flaw sizes have no practical interest for a defect tolerance analysis since the 0.65 mm size is about one third of the tube thickness

The theoretical S-N curves given by equation (10) are plotted in Figs. 12 and 13 together with the experimental data obtained in the welded tubes (not precracked). Two sets of curves were obtained corresponding to $f(\alpha)$ given by equation(5)or by the K calibration obtained with equations 7a and 7b. For both rectangular and square tubes the Murakami solution for $f(\alpha)$ gives higher fatigue strengths and the difference increases with the initial flaw size. However the difference is increasing with the initial flaw size due to the N_3 term contribution for the total number of cycles. Hence, for high initial flaw sizes, N_3 is closer to N_1+N_2 and any differences in $f(\alpha)$ in equation (11.c) produce a larger variation in N_3.
Figure 12 is the plot for the rectangular tubes, which shows that fatigue strength is greater in the St 44-2 steel compared with St 46-2. The same behaviour was observed in the square tubes (Fig.13). Comparing the experimental S-N curves for the rectangular and square tubes no influence of geometry is detected. Hence both square and rectangular tubes have similar fatigue strengths.

Good agreement was obtained between the theoretical and experimental S-N curves. The slopes of the curves are very close thus indicating that the crack initiation period is small. The difference in fatigue strength between the St-44 and St 46 steels is mainly due to weld quality levels(initial flaw sizes). Thus, while for St 44-2 the initial flaw size level is between 0.1 and 0.2 mm, in the St 46-2 the experimental S-N curve lies close to the

0.65 mm initial flaw size curve. This is confirmed by the position of the experimental S-N curve in the 0.65 mm precracked specimens, in the scatter band of the St 46-2 S-N curves in plain as welded specimens, (Figs. 12 and 13). Hence fatigue life is greatly dependent on the initial flaw sizes and good fatigue strength is obtained if the defect tolerance level is kept below 0.1 to 0.2 mm. If these limits are increased up to 0.65 mm as in the St 46-2 steel tubes fatigue strength is reduced by a factor of 2/3 and a fatigue limit may not be obtained (Fig.12 and 13). However for the results in the St 44-2 steel tubes a fatigue limit may be defined with a value between 160 to 170 MPa. For the St 46-2 tubes perhaps it is possible to define a fatigue limit close to 120 MPa (Figs.12 and 13).

CONCLUSIONS

1. Fracture Mechanics can be applied sucessfully in the fatigue analysis of welded rectangular thin walled tubes used in bus structures.

2. A stress intensity factor formulation was derived to obtain the stress intensity values for cracks propagating in the top or bottom faces of the tube and in the lateral sides.

3. S-N data was obtained to establish appropriate design stresses and to compare the influence on fatigue life of steel grade and tube geometry

4. Fractographic analysis has revealed that the fatigue cracks are usually initiated at the tube corner in the weld toe and then propagated in the horizontal and lateral side. The main microstructural crack propagation modes were identified and compared.

5. Theoretical crack propagation S-N curves were derived based on the stress intensity factor equations mentioned in 2 and using the Paris law equation for the material and geometry of the tubes. These curves can be applied in the defect tolerance analysis of the structure since good agreement was found with the appropriate experimental S-N curves.

6. Further work is required to improve the stress intensity model using 3D finite element nodes. The experimental work should be extended to other tube thicknesses and weld details.

REFERENCES

1. Ferreira, J.A., Branco, C.M. and Radon, J.C., "Fatigue crack growth in welded steel rectangular hollow sections", Proc. Int. Conf. Fracture mechanics technology applied to material evaluation and structure design, Melbourne, Australia, August 1982

2. Ferreira, J.A., Branco, C.M. and Radon, J.C., Fatigue behaviour of steel rectangular hollow sections used in bus structures, Ibid, 1982

3. Branco, C.M., Fatigue design of bus structures, Proc. Int. Conf. on structure failure, product liability and technical insurance, Viena, Austria, September 1983

4. Ferreira, J.A., Branco, C.M. and Radon, J.C., Fatigue life assessment in transport vehicles, Proc. Int. Conf. on Fracture prevention in energy and transport systems, Rio de Janeiro, Brasil, Nov. /Dec. (1983)

5. Wardenier, J. and Dutta, D. The fatigue behaviour of lattice girder joints in square hollow sections, Proc. Int. Conf. on Joints in Structural Steelwork, Teeside, April 6-9, (1981)

6. Wardenier, J.,"Hollow Section Joints", (Delft University Press, Delft, Holland, 1982)

7. Stephens, R.I. and Glinka, G.,"Experimental determination of K for surface cracks in a square tube under torsion, Exp. Mech.,24, 1980

8. Mc. Dermott, M.E. and Stephens, R.I., "Experimental determination of K for hollow rectangular tubes containing corner cracks", Fracture Mechanics, ASTM STP 677,(1979),719

9. Matoba,M., Kawasaki, T., Fujii, T. and Yamauchi, T., Evaluation of fatigue strength of welded steel structures hull's members, hollow section joints, piping and vessel joints, Doc. IIW-XIII-1082-83, International Institute of Welding, 1983

10. IRSID, Institut de Recherches de la Sidérurgie Française, Proc. Conf. Int. L'Acier dans les Structures marines, Paris, France, 1981

11. Albrecht, P. and Yamada, K., Rapid calculation of stress intensity factors, J.Est.Division, Proc. ASCE, 103, (1977), 377

12. Tada, K.,Paris, P.C. and Irwin, G.R., "The Stress Analysis of Cracks Handbook", Del Research Corporation, USA, 1973

13. Gurney, T.R., "Fatigue of Welded Structures", (Cambridge University Press, England, 1979)

14. Fernandes, A.A., Branco, C.M., Castro, P.T. and Oliveira, F.,Fatigue crack propagation in thin hollow steel sections, Proc. Int. Conf on Fracture prevention in energy and transport systems, Rio de Janeiro, Brasil, Nov./Dec.(1983)

15. Murakami, Y., "Analysis of mixed mode stress intensity factors by body force methods", in Numerical Methods in Fracture Mechanics, (Pineridge Press, England, 1980)

ACKNOWLEDGEMENTS

This work is sponsored jointly by JNICT (Portuguese National Council for Scientific and Technological Research) under the research contract 409.82.18 and also by Salvador Caetano IMVT, SARL to whom the authors acknowledge the support. Thanks are also due to Mr. Pedro Matos who conducted part of the fatigue tests and Dr.John Radon for very interesting and stimulating discussions.

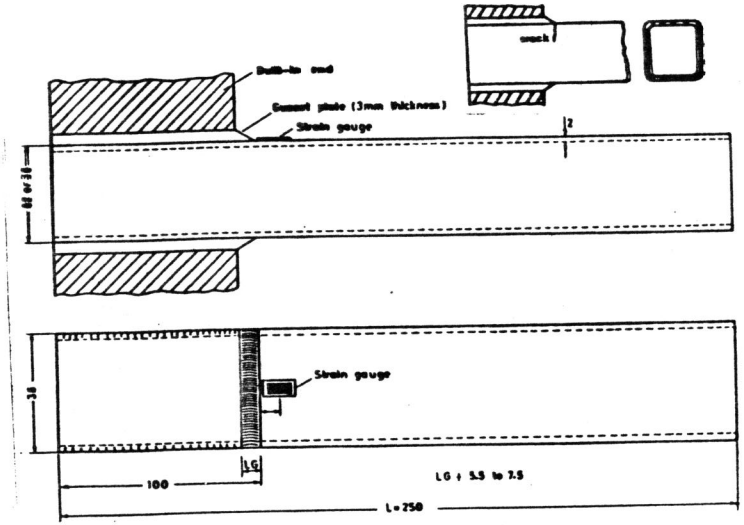

Figure 1 Tubular specimen with a fillet welded gusset plate used in the experimental programme

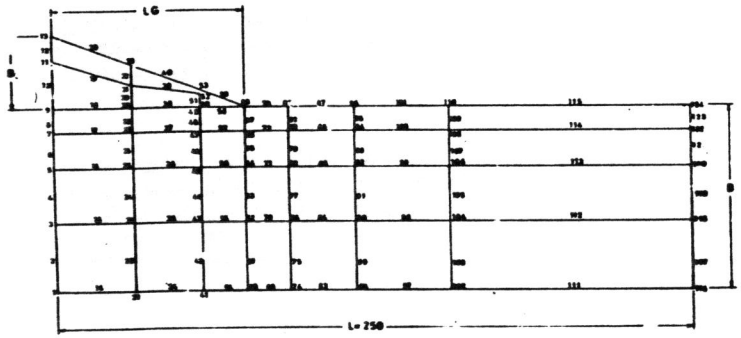

Figure 2 Finite element mesh for stress computation in the upper part of the tube

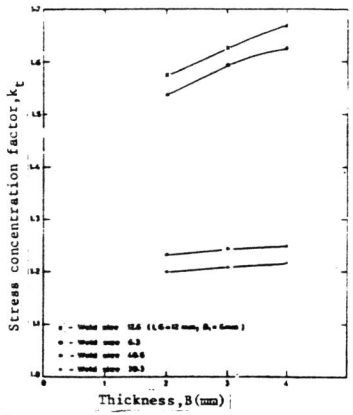

Figure 3 Variation of K_t with B as a function of LG and B_1

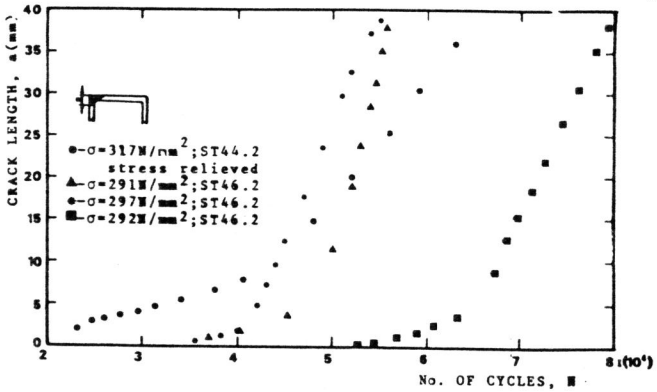

Figure 4 Crack propagation curve in welded tubes 82x38x2 with a 0.65 mm deep notch. Cantilever bending. R=0

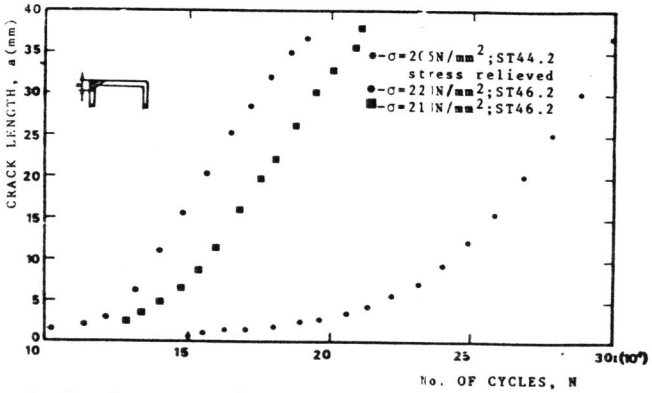

Figure 5 Crack propagation curve in welded tubes 82x38x2 with a 0.65 mm deep notch. Cantilever bending. R=0

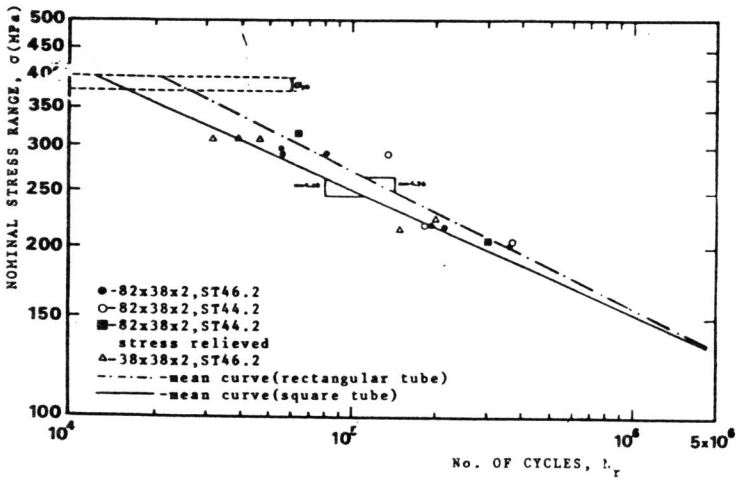

Figure 6 Experimental S-N curve in welded rectangular and square tubes with a 0.65 mm deep notch. Cantilever bending. R=0

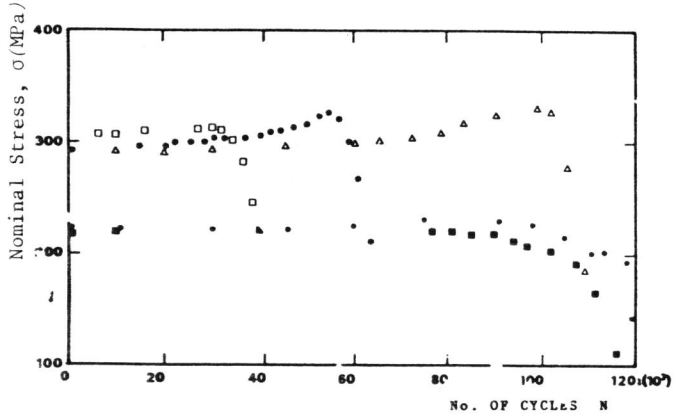

Figure 7 Typical variation of nominal stress with the number of cycles. Tubes 82x38x2 and 38x38x2

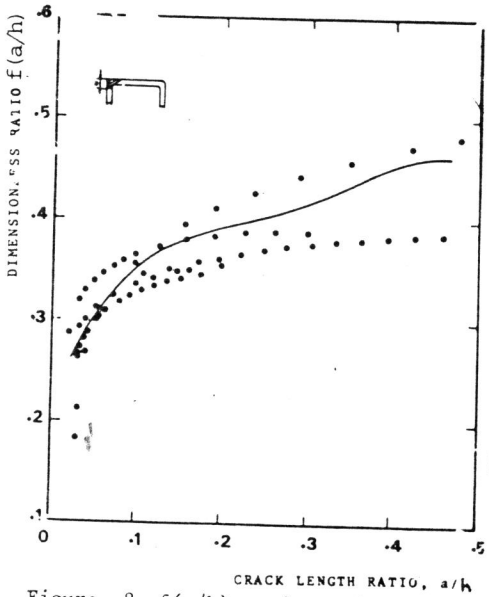

Figure 8 f(a/h) against a/h for rectangular tubes (82x38x2).St 46-2 steel

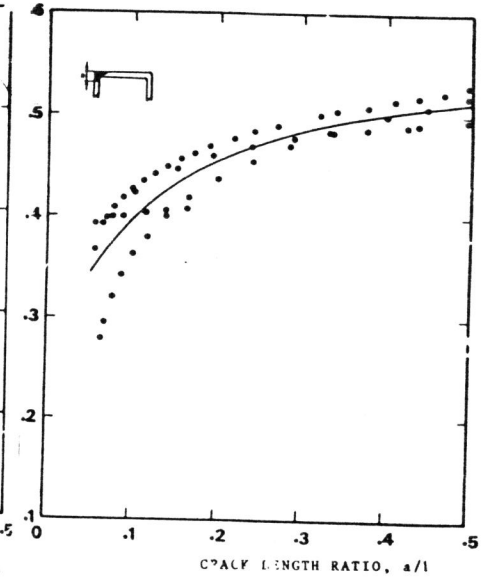

Figure 9 f(a/h) against a/h for square tubes(38x38x2).St 46-2 steel

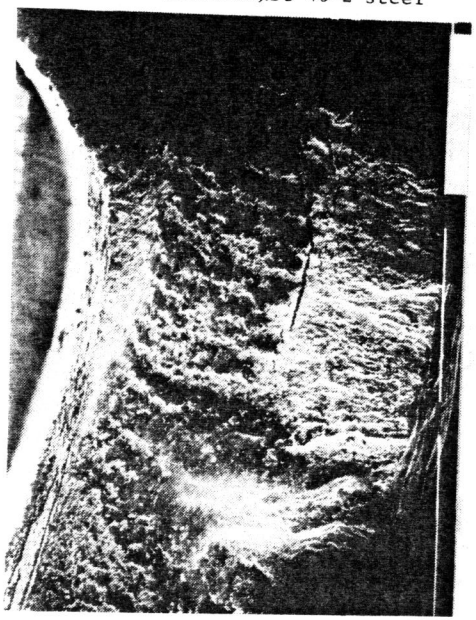

Figure 10 Fracture surface showing crack initiation in the top left of a square tube(35x Magnification)

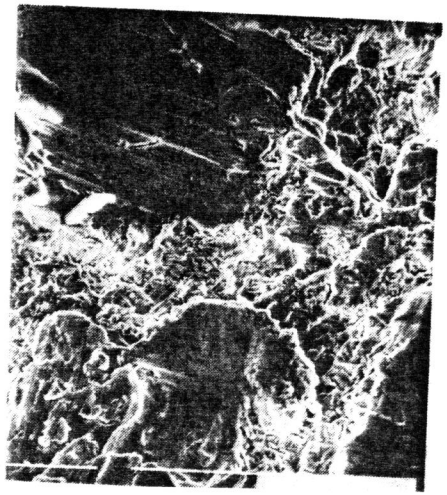

Figure 11 Mixed mode of crack propagation in the lateral side of a tube, in St 46-2 steel(500x Magnification)

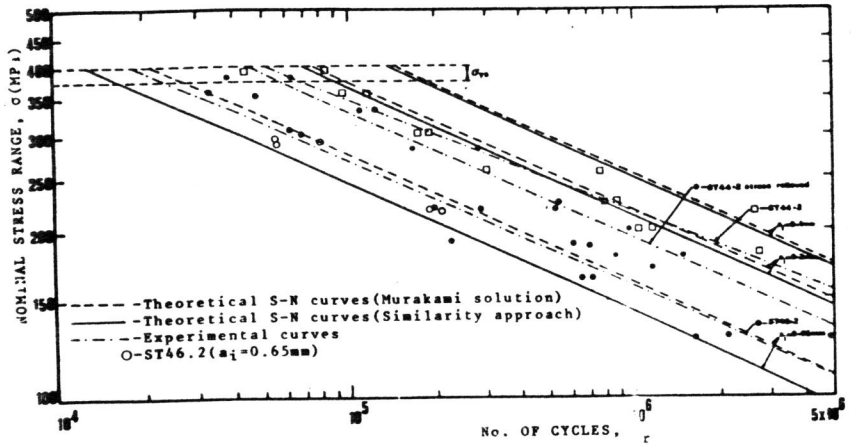

Figure 12 Theoretical and experimental S-N curves for the welded rectangular tubes (82x38x2) of St 44-2 and St 46-2 steel. R=0. Cantilever bending

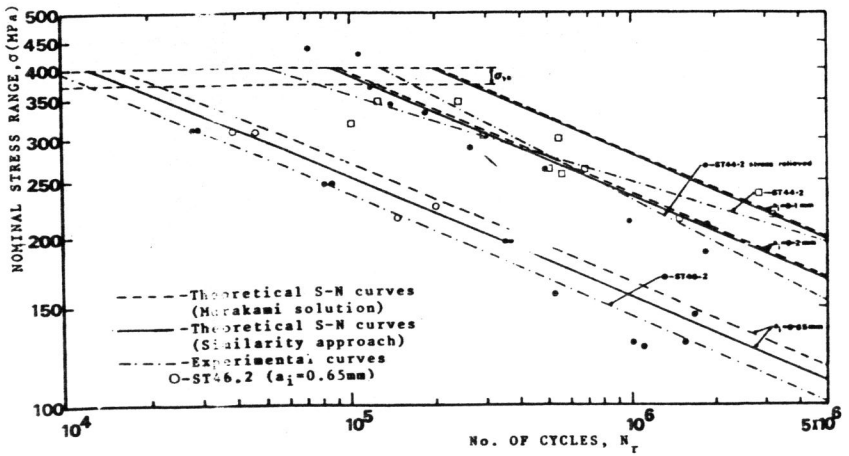

Figure 13 Theoretical and experimental S-N curves for the welded square tubes (38x38x2)of St 44-2 and St 46-2 steels. R=0. Cantilever bending